# OPTIMAL HAAR WAVELET DECOMPOSITIONS
# ON SPHERICAL SOUND FIELDS

Kensuke Fujinoki

Department of Mathematical Sciences
Tokai University
4-1-1 Kitakaname, Hiratsuka, Kanagawa 259-1292, Japan
fujinoki@tokai-u.jp

Abstract. *To represent the sound field of a sphere, optimal parameter values for a set of spherical Haar wavelets forming an orthogonal basis are investigated. The Haar wavelet basis is defined on a sphere, which is sampled using a triangular mesh. Results from numerical experiments yield optimal parameter values that minimize the distortion error of the nonlinear approximation for various sound fields generated using sinusoidal waves of different frequencies.*
**Keywords:** Wavelet, Sphere, Sound field

1. **Introduction.** Signals that can be spherically parameterized are found in a wide range of scientific fields including astronomy, geoscience, fusion physics, and medical imaging. An efficient representation for spherical signals is therefore important, especially when large data sets need to be compressed. The classical standard approaches for the representations of a function or data on a sphere are the spherical harmonics and the spherical radial basis functions.

Wavelet-based approaches have recently been developed and proven to be useful tools for representing spherical signals, including the discrete wavelet transform based on the triangulation of a sphere [1, 2, 3, 4]. A notable example is the orthogonal Haar wavelets on a sphere proposed in [5, 6] because it offers a means to construct a variety of orthogonal systems. These types of wavelets have various applications in areas such as the analysis of fluid flow [2], the texture of crystals [7], the cosmic microwave background [8], and image inpainting [9].

Applied to fluid analysis, wavelets have a three-dimensional structure [10, 11]. From the area of acoustic engineering, sound fields reflect a similar structure to fluids. They represent spatial information carried by sound, and its preservation, reproduction, and evaluation which includes the scattering analysis of sound [12] are one of the main topics of acoustic engineering.

A spherical sound field is often used in simulation models to treat the three-dimensional structure associated with the distribution of sound because its geometrical features can simply be expressed and all sound is composed of spherical waves. In general, because sound fields essentially fill the available three-dimensional space, which can be relatively huge, the amount of data required to express it is enormous. Therefore, an efficient representation of the spherical sound field is required.

Our study aims to develop an efficient method for representing spherical sound fields by means of wavelets. In this paper, we focus on the orthogonal Haar wavelets on a sphere given by Rosca [5, 6], and construct optimal basis functions for representing spherical sound fields appropriate for various situations.

This paper is organized as follows. The following section provides a preliminary introduction of our sphere and its triangulation, which sets the stage for our formulation.

Section 3 introduces sets of the Haar wavelets on the sphere, showing that several parameters are required in constructing the spherical Haar wavelets. Section 4 gives fast computational algorithms for a spherical signal. Our results from numerical experiments are presented in Section 5, and we derive optimal parameter values for the spherical Haar wavelets in the nonlinear approximation of the acoustic pressure of the spherical sound fields. Section 6 gives conclusions.

2. **Spherical Triangulations.** Following Rosca's formulation, we introduce a triangulation of a sphere and spherical Haar wavelets. Let $\mathbb{S}^2 = \{\boldsymbol{\eta} = (\eta_1, \eta_2, \eta_3) \in \mathbb{R}^3; \eta_1^2 + \eta_2^2 + \eta_3^2 = 1\}$ be a two-dimensional unit sphere. Let $\Pi \subset \mathbb{R}^3$ be a convex manifold that has $n$ triangular faces $T_n$. We denote by $\mathcal{T}_0 = \{T_i\}_{i=0}^{n-1}$ the set of faces of $\Pi$. We also define the surface of $\Pi$ by $\Omega \ni (x_1, x_2, x_3) = \boldsymbol{x}$.

The radial projection onto $\mathbb{S}^2$, $p : \Omega \to \mathbb{S}^2$ is written by

$$p(\boldsymbol{x}) = \frac{\boldsymbol{x}}{\|\boldsymbol{x}\|}, \quad \boldsymbol{x} \in \Omega.$$

Its inverse projection $p^{-1} : \mathbb{S}^2 \to \Omega$ is defined by

$$p^{-1}(\boldsymbol{\eta}) = \frac{-d}{a\eta_1 + b\eta_2 + c\eta_3} \boldsymbol{\eta}, \quad \boldsymbol{\eta} \in \mathbb{S}^2,$$

where $ax_1 + bx_2 + cx_3 + d = 0$.

We assume that $\Pi$ is an icosahedron, which has $n = 20$ faces, and consider its triangulation in $\Omega$ as $\{\mathcal{T}_j\}_{j \in \mathbb{Z}_+}$, where $\mathbb{Z}_+ = \{j \in \mathbb{Z}; j \geq 0\}$. Let $[M_1 \, M_2 \, M_3] \subset \Omega$ be one of the triangles in $\mathcal{T}_0$ and $[A_1 \, A_2 \, A_3]$ be the midpoint of the edges $M_2 M_3$, $M_3 M_1$, and $M_1 M_2$, respectively. We then define a new set

$$\mathcal{T}_1 = \bigcup_{[M_1 \, M_2 \, M_3] \in \mathcal{T}_0} \{[M_1 \, A_2 \, A_3], [A_1 \, M_2 \, A_3], [A_1 \, A_2 \, M_3], [A_1 \, A_2 \, A_3]\},$$

which is a finer collection of 4-divided triangles of $\mathcal{T}_0$. By iterating this process, we obtain a triangulation $\mathcal{T}_j$ of $\Omega$. The triangulation can also be written by $\mathcal{T}_j = \{T_{j,k}\}_{k \in \mathcal{K}_j}$, where $\mathcal{K}_j = \{0, 1, 2, \dots, n \cdot 4^j - 1; j \in \mathbb{Z}_+\}$ is an index set for the 4-divided triangles at each level $j$. Note that $\{T_{j,k}\}_{k \in \mathcal{K}_j}$ is a disjoint set that contains only edges of the triangles each other. The number of triangular faces in $\mathcal{T}_j$ is $|\mathcal{T}_j| = n \cdot 4^j$.
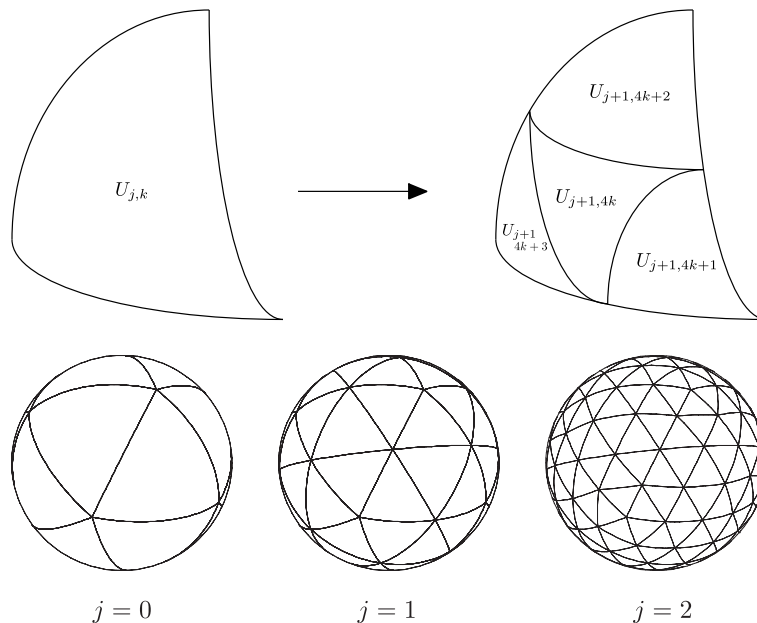


FIGURE 1. Triangulation of a sphere

In a similar way, we next consider a triangulation of $\mathbb{S}^2$. We define the projection of $\mathcal{T}_j$ onto $\mathbb{S}^2$ by $\mathcal{U}_j = \{p\,(T_{j,k})\,; T_{j,k} \in \mathcal{T}_j\}$. As for the surface $\Omega$, this triangulation can be written as $\mathcal{U}_j = \{U_{j,k}\}_{k \in \mathcal{K}_j}$, and the number of disjoint spherical triangles $U_{j,k}$ is $|\mathcal{U}_j| = n \cdot 4^j$. The whole sphere $\mathbb{S}^2$ can be covered by $\mathcal{U}_j$ (see Figure 1).

3. **Spherical Haar Wavelets.** For a given $U_{j,k} \in \mathcal{U}_j$, we define a piecewise constant function $\phi_{U_{j,k}} : \mathbb{S}^2 \to \mathbb{R}$ by

$$
\phi_{U_{j,k}}(\boldsymbol{\eta}) = \begin{cases} 1, & \boldsymbol{\eta} \text{ is inside } U_{j,k}, \\ 1/2, & \boldsymbol{\eta} \text{ is on the edges of } U_{j,k}, \\ 0, & \boldsymbol{\eta} \notin U_{j,k}. \end{cases}
$$

We call it the spherical Haar scaling function. As $\mathcal{U}_j \subset \mathcal{U}_{j+1}$, the spherical triangles $U_{j,k}$ are defined by their refined triangles $U_{j+1,k}$. The spherical Haar scaling function therefore satisfies the dilation equation

$$
\phi_{U_{j,k}}(\boldsymbol{\eta}) = \sum_{\ell=0}^{3} \phi_{U_{j+1,4k+\ell}}(\boldsymbol{\eta}).
$$

The energy of the scaling function at the coarsest level is normalized to 1. From the definition, the support of $\phi_{U_{j,k}}$ immediately follows, supp $\phi_{U_{j,k}} = U_{j,k}$. If $k, \ell \in \mathcal{K}_j$ and $k \neq \ell$, each support of the scaling functions is disjoint because supp $\phi_{U_{j,k}} \cap$ supp $\phi_{U_{j,\ell}}$ is the empty set or an edge of $U_{j,k}$. Moreover, the measure is zero. Therefore, the scaling function is orthogonal in the sense that

$$
4^j \left\langle \phi_{U_{j,k}}, \phi_{U_{j,\ell}} \right\rangle_{\mathbb{S}^2} = \delta_{k,\ell}, \quad \text{for } k, \ell \in \mathcal{K}_j \text{ and } j \in \mathbb{Z}_+,
$$

where $\langle f, g \rangle_{\mathbb{S}^2}$ is the inner product for $f, g \in L^2(\mathbb{S}^2)$, and $\delta_{k,\ell}$ is the Kronecker delta defined by

$$
\delta_{k,\ell} = \begin{cases} 1, & \text{if } k = \ell, \\ 0, & \text{otherwise.} \end{cases}
$$

We next consider wavelet functions that are associated functions of the scaling function on the sphere. The straightforward generalization of the multiresolution analysis (MRA) shows that there are three wavelets $\left\{\psi_{U_{j,k}}^m\right\}_{m=1,2,3}$, which are defined by a system of equations

$$
\begin{pmatrix} \phi_{U_{j,k}} \\ \psi_{U_{j,k}}^1 \\ \psi_{U_{j,k}}^2 \\ \psi_{U_{j,k}}^3 \end{pmatrix} = \begin{pmatrix} 1 & 1 & 1 & 1 \\ \alpha_1 & \beta & \alpha_2 & \gamma \\ \alpha_2 & \beta & \gamma & \alpha_1 \\ \gamma & \beta & \alpha_1 & \alpha_2 \end{pmatrix} \begin{pmatrix} \phi_{U_{j+1,4k}} \\ \phi_{U_{j+1,4k+1}} \\ \phi_{U_{j+1,4k+2}} \\ \phi_{U_{j+1,4k+3}} \end{pmatrix} \tag{1}
$$

with $\alpha_1, \alpha_2, \beta, \gamma \in \mathbb{R}$. The supports of $\psi_{U_{j,k}}^m$ are similar to $\phi_{U_{j,k}}$, namely, supp $\psi_{U_{j,k}}^m = U_{j,k}$ for $m = 1, 2, 3$, and for $k \neq \ell$, supp $\psi_{U_{j,k}}^m \cap$ supp $\psi_{U_{j,\ell}}^n = \emptyset$ or an edge.

To determine the parameters $\alpha_1$, $\alpha_2$, $\beta$, and $\gamma$, we assume that the scaling function and the wavelets are orthogonal for $k, \ell \in \mathcal{K}_j$ and $m, n = 1, 2, 3$, in the sense that

$$
\left\langle \psi_{U_{j,k}}^m, \phi_{U_{j,\ell}} \right\rangle_{\mathbb{S}^2} = 0 \text{ and } 4^j \left\langle \psi_{U_{j,k}}^m, \psi_{U_{j',\ell}}^n \right\rangle_{\mathbb{S}^2} = \delta_{j,j'} \delta_{k,\ell} \delta_{m,n}. \tag{2}
$$

The orthogonal condition (2) yields $\gamma = -(\beta + \alpha_1 + \alpha_2)$ and $\beta = \pm 1/2$. For $\beta = 1/2$, matrix (1) becomes

$$M_{\beta_+} = \begin{pmatrix} 1 & 1 & 1 & 1 \\ \alpha_1 & \dfrac{1}{2} & \alpha_2 & -\left(\dfrac{1}{2}+\alpha_1+\alpha_2\right) \\ \alpha_2 & \dfrac{1}{2} & -\left(\dfrac{1}{2}+\alpha_1+\alpha_2\right) & \alpha_1 \\ -\left(\dfrac{1}{2}+\alpha_1+\alpha_2\right) & \dfrac{1}{2} & \alpha_1 & \alpha_2 \end{pmatrix}.$$

For $\beta = -1/2$, we obtain a matrix similar to the above having different signs:

$$M_{\beta_-} = \begin{pmatrix} 1 & 1 & 1 & 1 \\ \alpha_1 & -\dfrac{1}{2} & \alpha_2 & \left(\dfrac{1}{2}-\alpha_1-\alpha_2\right) \\ \alpha_2 & -\dfrac{1}{2} & \left(\dfrac{1}{2}-\alpha_1-\alpha_2\right) & \alpha_1 \\ \left(\dfrac{1}{2}-\alpha_1-\alpha_2\right) & -\dfrac{1}{2} & \alpha_1 & \alpha_2 \end{pmatrix}.$$

Hence, an orthogonal basis of the spherical Haar wavelets is determined by

$$E_1 = 4\left(\alpha_1^2 + \alpha_1\alpha_2 + \alpha_2^2\right) + 2(\alpha_1 + \alpha_2) - 1 = 0, \text{ for } \beta = 1/2, \tag{3}$$

$$E_2 = 4\left(\alpha_1^2 + \alpha_1\alpha_2 + \alpha_2^2\right) - 2(\alpha_1 + \alpha_2) - 1 = 0, \text{ for } \beta = -1/2. \tag{4}$$

Figure 2 depicts ellipses $E_1$ and $E_2$ that represent (3) and (4), respectively. For ellipse $E_1$, the intervals for $\alpha_i$, $i = 1, 2$ are $\alpha_i \in [-5/6, 1/2]$, whereas for ellipse $E_2$, the intervals are $\alpha_i \in [-1/2, 5/6]$. Any pair of $(\alpha_1, \alpha_2)$ gives an orthogonal system of spherical Haar wavelets including the results obtained in [2, 4]. For example, choosing $\alpha_1 = \alpha_2 = 1/6$
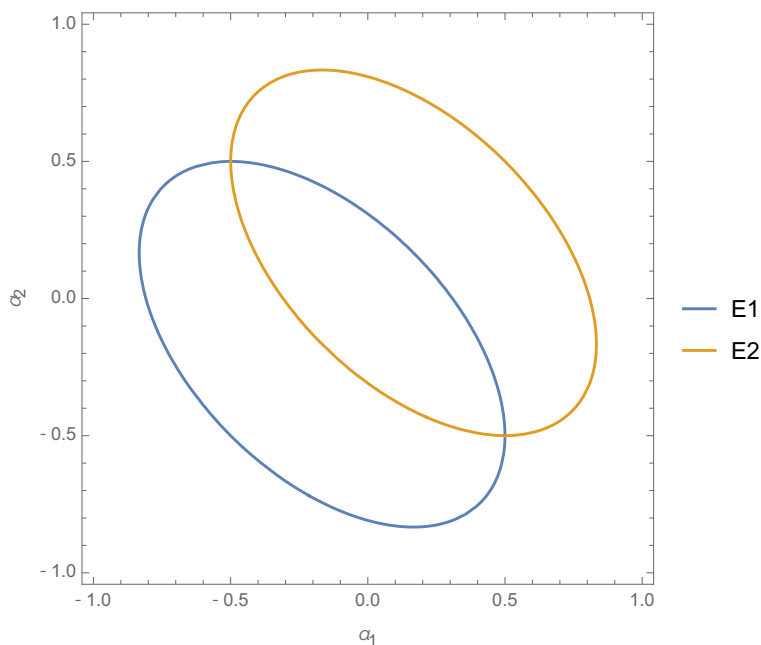


FIGURE 2. Equations $E_1$ and $E_2$

gives

$$M_{\beta_+} = \frac{1}{2} \begin{pmatrix} 1 & 1 & 1 & 1 \\ 1/3 & 1 & 1/3 & -5/3 \\ 1/3 & 1 & -5/3 & 1/3 \\ -5/3 & 1 & 1/3 & 1/3 \end{pmatrix}, \tag{5}$$

and for $\beta = \alpha_1 = 1/2$ gives

$$M_{\beta_+} = \frac{1}{2} \begin{pmatrix} 1 & 1 & 1 & 1 \\ -1 & 1 & -1 & 1 \\ -1 & 1 & 1 & -1 \\ 1 & 1 & -1 & -1 \end{pmatrix}.$$

Note that the coefficients for $\phi_{U_{j,k}}$ are normalized to $1/2$ so that the system satisfies the orthogonality condition $M_{\beta_+} M_{\beta_+}^T = M_{\beta_+}^T M_{\beta_+} = I$, where $I$ is the identity matrix.

4. **Spherical Wavelet Transform.** The MRA underlies the fundamental structure of the discrete wavelet transform (DWT) [13]. A straightforward application of the MRA to $\mathbb{S}^2$ produces a nested sequence of spaces $\{\mathcal{V}_j\}_{j \in \mathbb{Z}}$:

$$\{0\} \to \cdots \subset \mathcal{V}_{j-1} \subset \mathcal{V}_j \subset \mathcal{V}_{j+1} \subset \cdots \to L^2\left(\mathbb{S}^2\right),$$

where the spaces $\mathcal{V}_j \subset L^2\left(\mathbb{S}^2\right)$, called approximation spaces, are spanned by the scaling function

$$\mathcal{V}_j = \overline{\text{Span}\{\phi_{j,k}(x)\}_{k \in \mathcal{K}_j}},$$

whereas the three wavelets generate the detail spaces

$$\mathcal{W}_j^m = \overline{\text{Span}\left\{\psi_{j,k}^m(x)\right\}_{k \in \mathcal{K}_j}}, \quad m = 1, 2, 3.$$

From (2), they are mutually orthogonal,

$$\mathcal{W}_j^m \perp \mathcal{W}_j^n \perp \mathcal{V}_j, \quad m \neq n,$$

implying that the space $\mathcal{V}_j$ splits,

$$\mathcal{V}_j = \mathcal{V}_{j-1} \oplus \mathcal{W}_{j-1}^1 \oplus \mathcal{W}_{j-1}^2 \oplus \mathcal{W}_{j-1}^3.$$

With the nested structure of the space $\mathcal{V}_j \subset \mathcal{V}_{j+1}$ and if $\bigcup_{j \in \mathbb{Z}_+} \mathcal{V}_j$ is dense in $L^2\left(\mathbb{S}^2\right)$, we then have the MRA of $L^2\left(\mathbb{S}^2\right)$.

In terms of a function $f_j \in \mathcal{V}_j$, this structure can be expressed as a decomposition of functions [14], written by

$$f_j(\boldsymbol{\eta}) = f_{j-1}(\boldsymbol{\eta}) + g_{j-1}^1(\boldsymbol{\eta}) + g_{j-1}^2(\boldsymbol{\eta}) + g_{j-1}^3(\boldsymbol{\eta}), \tag{6}$$

where

$$f_j(\boldsymbol{\eta}) = \sum_{k \in \mathcal{K}_j} \left\langle f, \phi_{U_{j,k}} \right\rangle_{\mathbb{S}^2} \phi_{U_{j,k}}(\boldsymbol{\eta}),$$

$$g_j^m(\boldsymbol{\eta}) = \sum_{k \in \mathcal{K}_j} \left\langle f, \psi_{U_{j,k}}^m \right\rangle_{\mathbb{S}^2} \psi_{U_{j,k}}^m(\boldsymbol{\eta}), \quad m = 1, 2, 3.$$

The orthogonal wavelet expansion of $f \in L^2\left(\mathbb{S}^2\right)$ is given by

$$f(\boldsymbol{\eta}) = \sum_{j,k,m \in \mathbb{Z}} \left\langle f, \psi_{U_{j,k}}^m \right\rangle_{\mathbb{S}^2} \psi_{U_{j,k}}^m(\boldsymbol{\eta}) = \sum_{j \in \mathbb{Z}_+} \sum_{m=1}^3 g_j^m(\boldsymbol{\eta}).$$

Let $\{c_{j,k}\}_{k \in \mathcal{K}_j}$ and $\left\{d_{j,k}^m\right\}_{k \in \mathcal{K}_j, m=1,2,3}$ be the approximation and detail coefficients defined by

$$c_{j,k} = \left\langle f, \phi_{U_{j,k}} \right\rangle_{\mathbb{S}^2}, \quad d_{j,k}^m = \left\langle f, \psi_{U_{j,k}}^m \right\rangle_{\mathbb{S}^2}.$$

Using (6), an approximation function $f_j \in \mathcal{V}_j$ can be decomposed into its coarser approximation function $f_{j-1} \in \mathcal{V}_{j-1}$ using

$$\sum_{k \in \mathcal{K}_j} c_{j,k} \phi_{U_{j,k}}(\boldsymbol{\eta}) = \sum_{k \in \mathcal{K}_j} c_{j-1,k} \phi_{U_{j-1,k}}(\boldsymbol{\eta}) + \sum_{m=1}^{3} \sum_{k \in \mathcal{K}_j} d_{j-1,k} \psi_{U_{j-1,k}}^m(\boldsymbol{\eta}),$$

which can be iterated to resolution level $J \leq j$. The reconstruction of $f_i \in \mathcal{V}_i$, $i > J$ is achieved by the summation

$$f_i(\boldsymbol{\eta}) = \sum_{k \in \mathcal{K}_j} c_{J,k} \phi_{U_{j,k}}(\boldsymbol{\eta}) + \sum_{j=J}^{i-1} \sum_{m=1}^{3} \sum_{k \in \mathcal{K}_j} d_{j,k}^m \psi_{U_{j,k}}^m(\boldsymbol{\eta}).$$

Let $\{h_k\}_{k \in \mathcal{K}_j}$ and $\{g_k^m\}_{k \in \mathcal{K}_j, m=1,2,3}$ be both real-valued filter coefficients, and set

$$M_{\beta_+} = \begin{pmatrix} h_0 & h_1 & h_2 & h_3 \\ g_0^1 & g_1^1 & g_2^1 & g_3^1 \\ g_0^2 & g_1^2 & g_2^2 & g_3^2 \\ g_0^3 & g_1^3 & g_2^3 & g_3^3 \end{pmatrix}.$$

Then the coefficients $\{c_{j,k}\}_{k \in \mathcal{K}_j}$ and $\left\{ d_{j,k}^m \right\}_{k \in \mathcal{K}_j, m=1,2,3}$ are calculated by applying the decomposition algorithm defined by

$$c_{j-1,k} = \sum_{\ell \in \mathcal{K}_j} h_{\ell-4k} c_{j,\ell}, \quad d_{j-1,k}^m = \sum_{\ell \in \mathcal{K}_j} g_{\ell-4k}^m c_{j,\ell}. \tag{7}$$

To recover a finer level of the coefficients, we use the reconstruction algorithm

$$c_{j,k} = \sum_{\ell \in \mathcal{K}_j} h_{k-4\ell} c_{j-1,\ell} + \sum_{m=1}^{3} \sum_{\ell \in \mathcal{K}_j} g_{k-4\ell}^m d_{j-1,\ell}^m.$$

5. **Numerical Experiments.** Various numerical experiments were performed to construct an optimal spherical Haar wavelet for a spherical sound field produced using sinusoidal waves at various frequencies. We assumed a free sound field of a sphere of radius $r = 1$ [m]. The point source $\boldsymbol{\zeta} \in \mathbb{R}^3$ is located outside the sphere. The distance from the sound source to an edge of the sphere is also 1 [m]. In this setting, the sound pressure generated with sinusoidal waves of different frequencies is given by

$$\Phi(\boldsymbol{\eta}) = \frac{-Ak \sin(\omega t - k\|\boldsymbol{\eta} - \boldsymbol{\zeta}\|)}{\|\boldsymbol{\eta} - \boldsymbol{\zeta}\|},$$

where $A \in \mathbb{R}$ is a constant, $k = \omega/c$ the wave number, and $c = 340$ [m/s] is the acoustic velocity. The level of triangulation is $j = 7$, which has $20 \cdot 4^7$ trixels. The frequencies selected were 0.5, 1, 2, 4, 8, and 16 [kHz] and the sampling frequency was set to 44.1 [kHz].

In choosing the parameter values of the orthogonal Haar system, we considered only $E_1$ because $E_1$ and $E_2$ produce essentially the same results; the difference is only a sign. Because $\alpha_2$ is given by $\alpha_1$,

$$\alpha_2 = \frac{1}{4}\left(-2\alpha_1 - 1 \pm \sqrt{-12\alpha_1^2 - 4\alpha_1 + 5}\right),$$

we determined the optimal pair $(\alpha_1, \alpha_2)$ on the ellipse $E_1$ that while changing the value of $\alpha_1 \in [-5/6, 1/2]$ minimizes the distortion error of our setting.

The distortion error is given by

$$\|\Phi - \Phi_M\|^2 = \sum_{(j,k,m) \notin I_M} \left| \left\langle \Phi, \psi_{U_{j,k}}^m \right\rangle_{\mathbb{S}^2} \right|^2,$$

where

$$\Phi_M(\boldsymbol{\eta}) = \sum_{(j,k,m)\in I_M} \left\langle \Phi, \psi_{U_{j,k}}^m \right\rangle_{\mathbb{S}^2} \psi_{U_{j,k}}^m(\boldsymbol{\eta}),$$

is the nonlinear approximation of $\Phi$ obtained using a selected set of coefficients,

$$I_M = \left\{ M \text{ largest coefficients of } \left\{ \left| \left\langle \Phi, \psi_{U_{j,k}}^m \right\rangle_{\mathbb{S}^2} \right| \right\}; j \in \mathbb{Z}_+, k \in \mathcal{K}_j, m = 1, 2, 3 \right\}.$$

The coefficients are calculated using the decomposition algorithm (7).

With the frequency set at 1 [kHz], the results for several sets of coefficient $I_M$, which contains $M$ largest coefficients of 100 [%] (original), 5 [%], and 1 [%], are shown in Figure 3. The parameter values $(\alpha_1, \alpha_2)$ that we chose are given in (5). We see an apparent increase in the distortion for decreasing values of the coefficients used for the nonlinear approximation. Despite its narrow support, we note that the spherical Haar wavelets still well represent the sound field even though the values of the coefficients are only 3 [%]. More details of the results are summarized in Table 1.



(a)            (b)            (c)
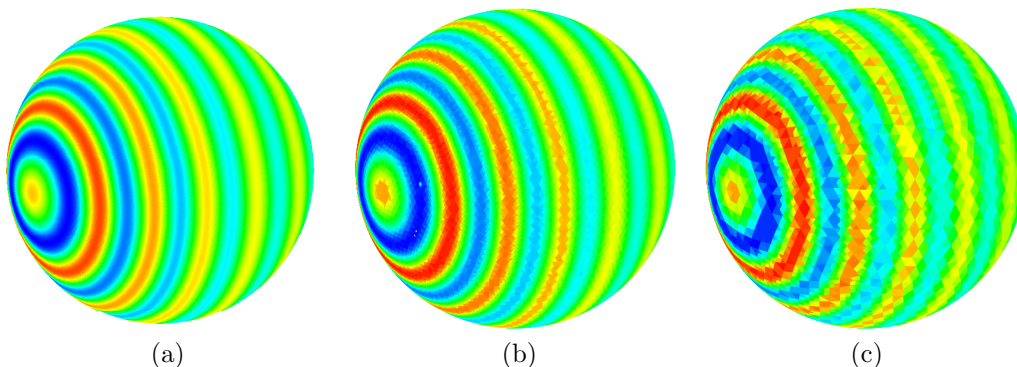
FIGURE 3. Nonlinear approximation of sound pressures $\Phi_M$ of sinusoidal waves at 1 [kHz] where $|I_M| = $ (a): 100 [%] (original), (b): 5 [%], (c): 1 [%]

TABLE 1. Distortion error $\|\Phi - \Phi_M\|^2$

| [kHz] \ [%] | 1 | 2 | 3 | 4 | 5 | 6 | 7 | 8 | 9 | 10 | Ave |
|---|---|---|---|---|---|---|---|---|---|---|---|
| 0.5 | $-5/6$ | $1/6$ | $-5/6$ | $1/6$ | $1/6$ | $-5/6$ | $-5/6$ | $1/6$ | $1/6$ | $1/6$ | $-5/6$ |
| 1 | $1/6$ | $-5/6$ | $1/6$ | $-5/6$ | $-5/6$ | $-5/6$ | $-5/6$ | $-5/6$ | $-5/6$ | $-5/6$ | $-5/6$ |
| 2 | $1/6$ | $-5/6$ | $1/6$ | $1/6$ | $1/6$ | $-5/6$ | $-5/6$ | $1/6$ | $-5/6$ | $-5/6$ | $1/6$ |
| 4 | $1/6$ | $-5/6$ | $-5/6$ | $-5/6$ | $-5/6$ | $-5/6$ | $-5/6$ | $-5/6$ | $-5/6$ | $-5/6$ | $-5/6$ |
| 8 | $-1/6$ | $0$ | $-5/6$ | $-5/6$ | $-5/6$ | $1/6$ | $-5/6$ | $-5/6$ | $1/6$ | $-5/6$ | $-5/6$ |
| 16 | $1/2$ | $-1/2$ | $-7/12$ | $-7/12$ | $-2/3$ | $-3/4$ | $1/3$ | $1/3$ | $1/4$ | $-5/6$ | $-3/4$ |

Table 1 gives the optimal $\alpha_1$ that minimizes the distortion error $\|\Phi - \Phi_M\|^2$ for both the coefficient ratio and the frequency. The results indicate the following trends. In almost every instance for coefficients $M$ and frequencies, the parameter values $\alpha_1 = -5/6$ or $\alpha_1 = 1/6$ are the best. These values do not depend on the coefficient ratio $M$. However, they depend on the frequency, especially at the higher frequency 16 [kHz]. This behavior can be explained using plots of the distortion errors as a function of $\alpha_1 \in [-5/6, 1/2]$; see Figure 4. In each figure, the bottom solid lines correspond to lower compression ratios whereas the top solid lines correspond to higher compression ratios. At lower frequencies, the curve representing the distortion has almost the same shape, but at the higher frequency 16 [kHz], its shape is inverted depending on the compression ratio. This implies that the optimal parameters of the spherical Haar wavelets change depending on the frequency component that the sound field contains.
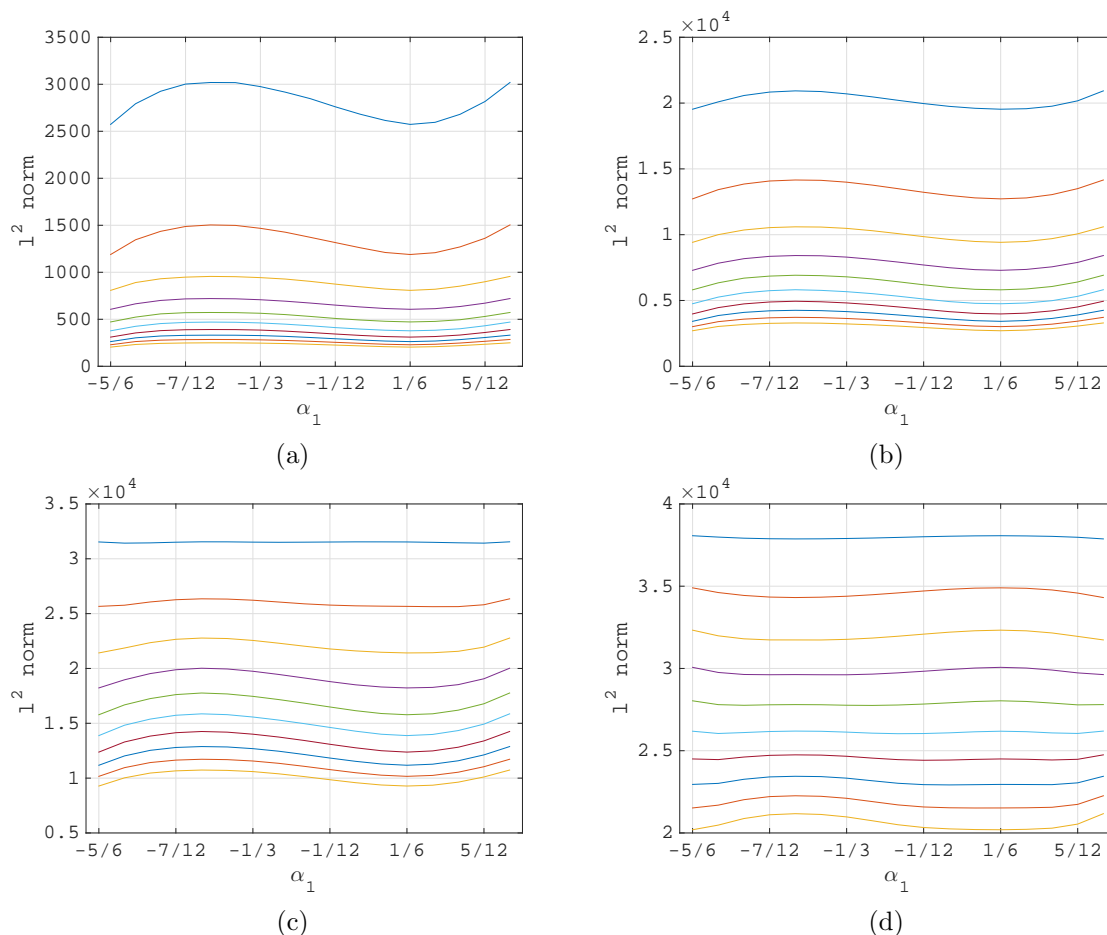
FIGURE 4. Distortion error $\|\Phi - \Phi_M\|^2$ at different $\alpha_1 \in [-5/6, 1/2]$ and different frequencies at (a): 1 [kHz], (b): 4 [kHz], (c): 8 [kHz], (d): 16 [kHz]. In each figure, the bottom solid lines represent lower compression ratios whereas the top solid lines represent higher compression ratios.

6. **Conclusions.** For representing a spherical sound field, we investigated the optimal parameter values of the orthogonal Haar wavelets on a sphere. In our numerical experiments, sound fields were produced with simple sinusoidal waves. We evaluated the performance of the nonlinear approximation using the spherical Haar wavelets and various combinations of parameter values. In summarizing our findings, there are two optimal values for the parameters, but the parameters depend on the frequency components of the sound fields, especially at high frequencies. These results are believed to be useful in representing a sound field that contains more complex frequency components.

To deal with a more realistic sound field, a smoother wavelet that has more support would be required such as those of [15, 16]. In addition, wavelets that can analyze not only spherical surfaces but also the interior of the sphere, where essentially the three-dimensional information is contained, are necessary and remain an open problem for future study.

**REFERENCES**

[1] P. Schröder and W. Sweldens, Spherical wavelets: Efficiently representing functions on the sphere, *Proc. of SIGGRAPH'95*, pp.161-172, 1995.

[2] G. Nielson, I. Jung and J. Sung, Haar wavelets over triangular domains with applications to multiresolution models for flow over a sphere, *Proc. of IEEE Visualization'97*, pp.143-150, 1997.

[3] M. Lounsbery, T. D. DeRose and J. Warren, Multiresolution analysis for surfaces of arbitrary topological type, *ACM Trans. Graphics*, vol.16, no.1, pp.34-73, 1998.

[4] G.-P. Bonneau, Optimal triangular Haar bases for spherical data, *Proc. of IEEE Visualization'99*, San Francisco, USA, pp.279-284, 1999.

[5] D. Rosca, Haar wavelets on spherical triangulations, in *Advances in Multiresolution for Geometric Modelling*, N. A. Dogson, M. S. Floater and M. A. Sabin (eds.), Springer, Berlin, 2005.

[6] D. Rosca, Optimal Haar wavelets on spherical triangulations, *Pure Math. Appl.,* vol.15, no.4, pp.429-438, 2006.

[7] H. Schaeben, D. Potts and J. Prestin, Spherical wavelets with application in preferred crystallographic orientation, *Proc. of IAMG'2001*, Cancun, 2001.

[8] P. Vielva, E. Martínez-González, R. B. Barreiro, J. L. Sanz and L. Cayón, Detection of non-Gaussianity in the Wilkinson microwave anisotropy probe first-year data using spherical wavelets, *Astrophysical Journal*, vol.609, pp.22-34, 2004.

[9] P. Abrial, Y. Moudden, J. Starck, J. Bobin, M. Fadili, B. Afeyan and M. Nguyen, Morphological component analysis and inpainting on the sphere: Application in physics and astrophysics, *J. Fourier Anal. and Appl.*, vol.13, no.6, pp.729-748, 2007.

[10] K. Kowal and A. Lazarian, Velocity field of compressible magnetohydrodynamic turbulence: Wavelet decomposition and mode scalings, *The Astrophysical Journal*, vol.720, no.1, pp.742-756, 2010.

[11] S. Grizzi and R. Camussi, Wavelet analysis of near-field pressure fluctuations generated by a subsonic jet, *Jounal of Fluid Mechanics*, vol.698, pp.93-124, 2012.

[12] D. K. Wilson, V. E. Ostashev, G. H. Goedecke and H. J. Auvemann, Quasi-wavelet calculations of sound scattering behind barriers, *Applied Acoustics*, vol.65, no.6, pp.605-627, 2004.

[13] S. Mallat, *A Wavelet Tour of Signal Processing*, 3rd Edition, Academic Press, 2008.

[14] K. Fujinoki, Biorthogonal wavelet expansions on the sphere, *Information*, vol.19, no.6(B), pp.2079-2088, 2016.

[15] F. Lanusse, A. Rassat and J. L. Starck, Spherical 3D isotropic wavelets, *Astronomy & Astrophysics*, vol.540, pp.1-11, 2012.

[16] P. Audet, Directional wavelet analysis on the sphere: Application to gravity and topography of the terrestrial planets, *Journal of Geophysical Research*, vol.116, pp.1-16, 2011.